

Design of Ambient Backscatter Training for Retrodirective Wireless Power Transfer

Sahar Idrees, *Student Member, IEEE*, Xiangyun Zhou, *Senior Member, IEEE*, Salman Durrani, *Senior Member, IEEE* and Dusit Niyato, *Fellow, IEEE*

Abstract

Wireless power transfer (WPT) using energy beamforming is a promising solution for low power devices in the future Internet of Things (IoT). In this work, we propose a WPT scenario with a retrodirective antenna at the energy transmitter (ET) and ambient backscatter at the energy receiver (ER). The retrodirective WPT at the ET eliminates the requirement of knowing the channel from the ET to ER, and the use of ambient backscattering (as opposed to active transmission) minimizes the energy consumption at the ER. We propose a training sequence design, i.e., the pattern of varying the reflection coefficient at the ER, to eliminate the direct-link interference from the ambient source. We show that when the ambient symbol duration is known, the ambient interference is fully cancelled by using the proposed design. We analytically model the system and derive a closed-form expression for the average harvested power at the ER, assuming that the retrodirective array size is large. Our results show that with practical parameter values, the proposed solution is robust to a small timing offset mismatch at the correlator and allows the ER to successfully harvest tens of μW of power, which is an important improvement for low-power IoT devices.

Index Terms

Ambient backscatter communication, retrodirective beamforming, training sequence design, wireless power transfer.

S. Idrees, X. Zhou and S. Durrani are with the Research School of Electrical, Energy and Materials Engineering, College of Engineering and Computer Science, The Australian National University, Canberra, ACT 2601, Australia (Emails: {sahar.idrees, xiangyun.zhou, salman.durrani}@anu.edu.au). D. Niyato is with the School of Computer Science and Engineering, Nanyang Technological University, 50 Nanyang Ave, Singapore 639798 (email: dniyato@ntu.edu.sg).

I. INTRODUCTION

A. Motivation and Related Work

The Internet of Things (IoT) is currently making a rapid transition from theory to practice. For instance, in Australia large scale IoT networks targeting smart cities [1], [2] and smart agriculture [3] are currently being deployed. As we move towards a world filled with a large number of IoT devices, the means to sustainably powering these IoT devices is a key challenge. In this regard, far-field wireless power transfer (WPT) is a promising technology to provide convenient wireless charging to low power IoT devices [4]–[7].

The problem of efficient WPT from an energy transmitter (ET) to an energy receiver (ER) has received much attention in the literature [8]–[17]. Typically, WPT relies on highly directional beamforming to increase the end-to-end power efficiency and overcome the severe radio frequency (RF) signal attenuation over distance. In this regard, different beamforming architectures have been proposed [8]–[10]. However, the implementation of these beamforming architectures requires channel state information (CSI) estimation at the ET [11], [12] or at the ER [13]–[16], or energy feedback from the ER to the ET [17], [18]. CSI estimation at the ER increases the complexity of the ER, which is undesirable. In addition, training methods suffer from high feedback overhead, which should also be avoided.

Recently, the use of a retrodirective array for WPT was proposed in [19] and [20]. A retrodirective array possesses a unique property of automatically responding to an incoming signal without prior knowledge regarding its angle of arrival [21]. Thus, it precludes the need for CSI estimation. A novel energy beamforming technique using a massive MIMO retrodirective antenna array at the ET was proposed in [19]. However, this scheme still required active signal transmission from the ER to initiate WPT, which consumes energy and may not be desirable for low power IoT devices. The active signal transmission from the ER to the ET was avoided in [22] by enabling the ER to backscatter the pilots emitted by the ET. However, conventional beamforming was still employed at the ET. A WPT scheme employing monostatic backscatter at the ER and a large retrodirective antenna at the ET was proposed in [20]. However, the charging request was initiated by the ET using active transmission.

Backscatter communication is a promising ultra-low power wireless communication paradigm, which eliminates the need for active transmission by the low power IoT devices [23], [24]. Conventional monostatic backscatter systems enable a tag to transmit to the reader by reflecting the RF signal sent by the reader itself. Recently, ambient backscatter which enables the tag to make use of ambient RF signals generated from ambient RF sources for communication has attracted a lot of attention [25]–[35]. A key issue in ambient backscatter communication systems is the direct-link interference that the RF ambient source causes to the tag. This is due to the fact that the ambient signals are omnipresent and much stronger than their backscattered versions. Numerous techniques have been used in the literature to address this issue of direct-link interference [27]–[35]. One approach is to consider this direct-link interference as a component of the background noise [27]–[29]. However, since the backscatter signal is very weak as compared to the ambient signal, such schemes do not perform so well. Other approaches involve general signal processing techniques [30]–[33] or backscatter specific solutions such as frequency shifting [34], [35]. In this regard, to the best of our knowledge, the use of Direct Sequence Spread Spectrum (DSSS) has not been considered to date.

B. Our Contributions

In this paper, we consider a WPT scenario between an ET equipped with a retrodirective antenna array and an ER equipped with an ambient backscatter tag. The fundamental signal recovery problem at the ET is then to recover the weak backscattered signal in the presence of strong direct-link ambient interference. In this context, our main contributions are:

- Taking inspiration from DSSS, we consider an ambient backscatter training scheme in which we vary the backscatter coefficient at the ER. This in effect multiplies the backscattered signal with a DSSS training signal and aims to capitalize on the spreading gain to boost the backscattered signal. We show that with a pseudo-noise (PN) training sequence, the average harvested power at the ER is small and it even reduces as the training period increases. This is due to the fact that the use of PN training sequence completely fails in dealing with the strong direct-link ambient interference.
- We then propose the design of the training sequence (i.e., the pattern of varying the reflection

TABLE I: Summary of Main Mathematical Symbols.

	Symbol	Description	Symbol	Description
System Parameters	α	Path-loss exponent	T_b	Duration of backscatter phase
	γ	Large scale channel attenuation	T_c	Duration in which backscatter coefficient remains constant
	β	Backscatter coefficient	T_s	Duration of one ambient symbol
	ζ	Energy harvesting efficiency	T_{off}	Duration of offset mismatch at the correlator
	σ_n^2	Variance of AWGN	M	Number of antennas at the ET
	d_1	Distance between the AS and the ER	N_c	Number of times backscatter coefficient switches during backscatter phase
	d_2	Distance between the ER and the ET	N_s	Number of ambient signals in one backscatter phase
	d_3	Distance between the AS and the ET	c_n	n -th chip in the training sequence
	P_s	Transmit power of the AS	P_t	Transmit power of the ET
RVs	s_i	i -th ambient symbol	\mathbf{f}	Channel from the ER to the ET
	g	Channel from the AS to the ER	\mathbf{r}_{ET}	Signal received at the ET during the backscatter phase
	\mathbf{h}	Channel from the AS to the ET	\mathbf{r}_{ER}	Signal received at the ER during PT phase

coefficient), to completely eliminate the direct-link ambient interference. We show that when the ambient symbol duration is known, the ambient interference is cancelled as long as there are equal number of $+1$ and -1 chips over one ambient symbol. The number of chips or equivalently the switching rate does not matter in this case. Hence, we can use the slowest switching rate, i.e., we can switch the backscatter coefficient only twice per ambient symbol period. We analytically model the system and derive a closed-form expression for the average harvested power at the ER. We show that this deterministic training sequence scheme has superior performance as compared to the PN training sequence scheme.

- Finally, we show that the proposed solution is robust to small timing offset mismatch at the correlator. This is because the undesired component is still perfectly eliminated. However, good synchronization is needed for the best performance. In addition, when the ambient duration is unknown, the power transfer performance under the proposed deterministic training scheme can be severely degraded. This is due to unequal durations of $+1$ and -1 chips in one ambient symbol. We show that in this mismatched case, the number of chips does matter, i.e., it is best to use a fast switching rate to minimize the effect of the uncanceled ambient.

C. Notation and Paper Organization

The following notation is used in this paper. $\Pr(\cdot)$ indicates the probability measure and $\mathbb{E}[\cdot]$ denotes the expectation operator. $f_X(x)$ denotes the probability density function (pdf) of a random variable X . For a complex valued vector \mathbf{v} , \mathbf{v}^* , \mathbf{v}^T and \mathbf{v}^H denote the conjugate, transpose and conjugate transpose, while the norm of the vector \mathbf{v} is given by $\|\mathbf{v}\| = \sqrt{\mathbf{v}^T \mathbf{v}}$. Finally, $G_p^m \begin{smallmatrix} n \\ q \end{smallmatrix} \left(\begin{smallmatrix} a_1, \dots, a_p \\ b_1, \dots, b_q \end{smallmatrix} \middle| z \right)$ represents the Meijer G-function [36]. A list of the main mathematical symbols employed in this paper is given in Table I.

The rest of the paper is organized as follows. Section II describes the system model and assumptions, along with the proposed wireless power transfer scheme and its phases. Section III presents the signal model of the system in terms of mathematical equations and states the metric of interest. Section IV gives the analysis of the proposed scheme with a PN sequence applied at the ER. Section V proposes the design of the deterministic training sequence for the elimination of the direct-link ambient interference and also gives the analysis of the system in this scenario, culminating in a closed form expression for average harvested power at the ER. Section VI deals with the impact of practical system aspects like imperfect synchronization at the correlator and change in ambient symbol duration. Finally, Section VI concludes the paper.

II. SYSTEM MODEL

We consider a WPT scenario with an ambient source (AS), an energy transmitter (ET) and an energy receiver (ER). The signal broadcasted from the AS is received by both the ET and the ER. We study the design of wireless power transfer (WPT) from the ET to the ER, as illustrated in Fig. 1.

The ER is a device (e.g., a sensor) that is capable of backscatter transmissions. It is composed of a single antenna element, a micro-controller, a variable impedance and an energy harvester. We also assume that the ER is equipped with an ideal energy storage element (e.g., a supercapacitor) for storing the energy transferred by the ET. The block diagram of the ER is illustrated in Fig. 2a.

The ET is connected to the power grid and transmits with a fixed power P_t using a large retrodirective antenna array. As mentioned earlier, the (digital) retrodirectivity means that the ET can re-transmit a signal back along the spatial direction of the incoming signal by conjugating its phase, without having to

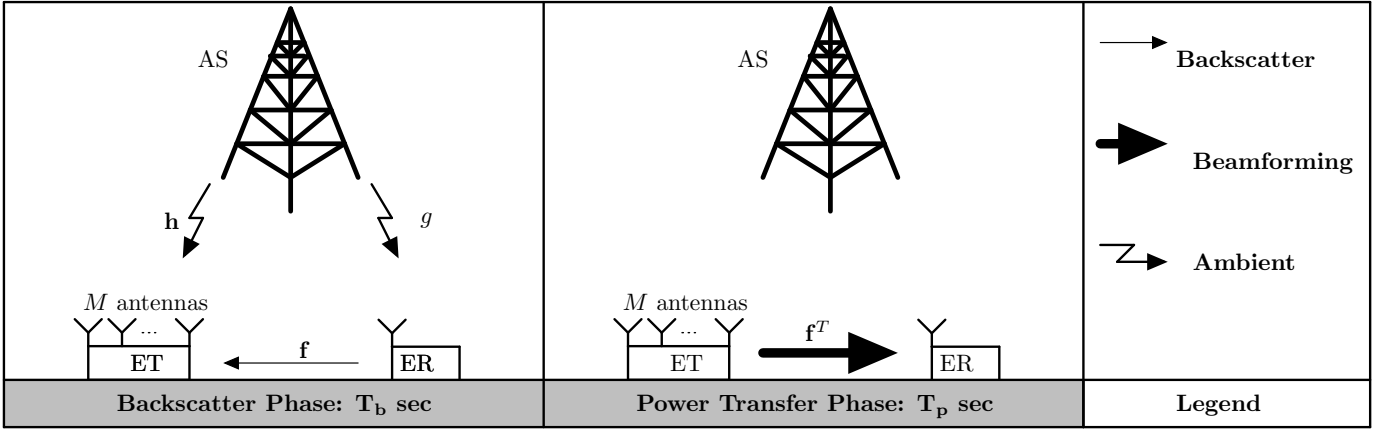


Fig. 1: Illustration of the system model.

calculate the direction of arrival [21], [37]. We assume that the number of antenna elements M at the ET is large. Thus, the ET forms a thin focussed beam when retrodirecting. The block diagram of the ET is illustrated in Fig. 2b.

A. Channel Assumptions

We assume that all the channel links are composed of large-scale path loss, with exponent α and statistically independent small-scale Rayleigh fading. We denote the distances between $AS \rightarrow ER$, $ER \rightarrow ET$ and $AS \rightarrow ET$ by d_1 , d_2 and d_3 respectively. Thus, large-scale attenuation is modelled as $\gamma_i = k_0(d_i/d_0)^{-\alpha}$ where k_0 is the constant attenuation for path-loss at a reference distance of d_0 and $i \in \{1, 2, 3\}$.

The $ER \rightarrow ET$, $AS \rightarrow ET$ and $AS \rightarrow ER$ fading channel coefficients, denoted by \mathbf{f} , \mathbf{h} and g respectively, are modeled as quasi-static and frequency non-selective parameters. Consequently, the complex fading channel coefficient g is a circular symmetric complex Gaussian random variable with zero mean and unit variance. Similarly, \mathbf{f} and \mathbf{h} are also uncorrelated circularly symmetric complex Gaussian random vectors, i.e., $\mathbf{f} = [f_1, \dots, f_M]^T \sim \mathcal{CN}(0, \mathbf{I}_M)$ and $\mathbf{h} = [h_1, \dots, h_M]^T \sim \mathcal{CN}(0, \mathbf{I}_M)$. We make the following assumptions regarding the channels:

- The fading channel coefficients are assumed to be constant over the duration of one set of backscatter and power transfer phases, i.e., $T_b + T_p$ seconds and independent and identically distributed from one $T_b + T_p$ slot to the next. The use of such channels is in line with the recent work in this research

field [19], [20], [38].

- We assume channel reciprocity, i.e., the channel from ER \rightarrow ET during the backscatter phase and the channel from ET \rightarrow ER during the power transfer phase are constant and transpose of each other [13]–[19].
- In this work, we do not need to make any channel state information (CSI) assumption. This is because the use of retrodirective antenna at the ET precludes the need for CSI.

B. Proposed Transmission Phases

The wireless power transfer from the ET to the ER takes place in two phases: (i) the backscatter phase and (ii) the power transfer phase, as shown in Fig. 1. During the first backscatter phase of duration T_b , the ER initiates a request for WPT by sending a backscattered ambient signal to the ET. During the second power transfer phase of duration T_p , the ET performs energy beamforming towards the ER. Note that in this work we will study the effect of varying the backscatter phase duration T_b , while we assume unit time in the power transfer phase.

1) *The Backscatter Phase:* The backscattering at the ER is achieved by adapting the level of the antenna impedance mismatch, which affects the power of the reflected signal. During the backscatter phase of duration T_b seconds, the switch in Fig. 2a stays in position 1 and the ER backscatters the ambient signal given by $r_b(t) = \sqrt{\gamma_1}g\beta s(t)$ where β is the backscatter reflection coefficient and $\sqrt{\gamma_1}gs(t)$ is the ambient signal arriving at the ER to be backscattered after suffering large scale attenuation γ_1 and channel coefficient g . In this work, we consider a BPSK-like backscatter coefficient having two different values, i.e., $\beta = \pm 1$.¹ The backscatter training means that the tag backscatters the ambient signal while switching the backscatter coefficient N_c times according to a pre-defined sequence between the values $+1$ and -1 at a rate of $\frac{1}{T_c}$, where T_c is the duration for which the backscatter coefficient maintains a certain value. This is effectively equivalent to multiplying the backscattered signal with a training signal $c(t)$ of N_c short duration pulses of amplitude $+1$ and -1 . Thus, at a given time instant t , the backscattered signal from the ER is given by $r_b(t) = \sqrt{\gamma_1}c(t)s(t)$, where γ_1 , g and $s(t)$ are as given above and $c(t)$ is the

¹ β can assume any pair of values $|\beta| \leq 1$. However, for simplicity we assume that $|\beta| = 1$.

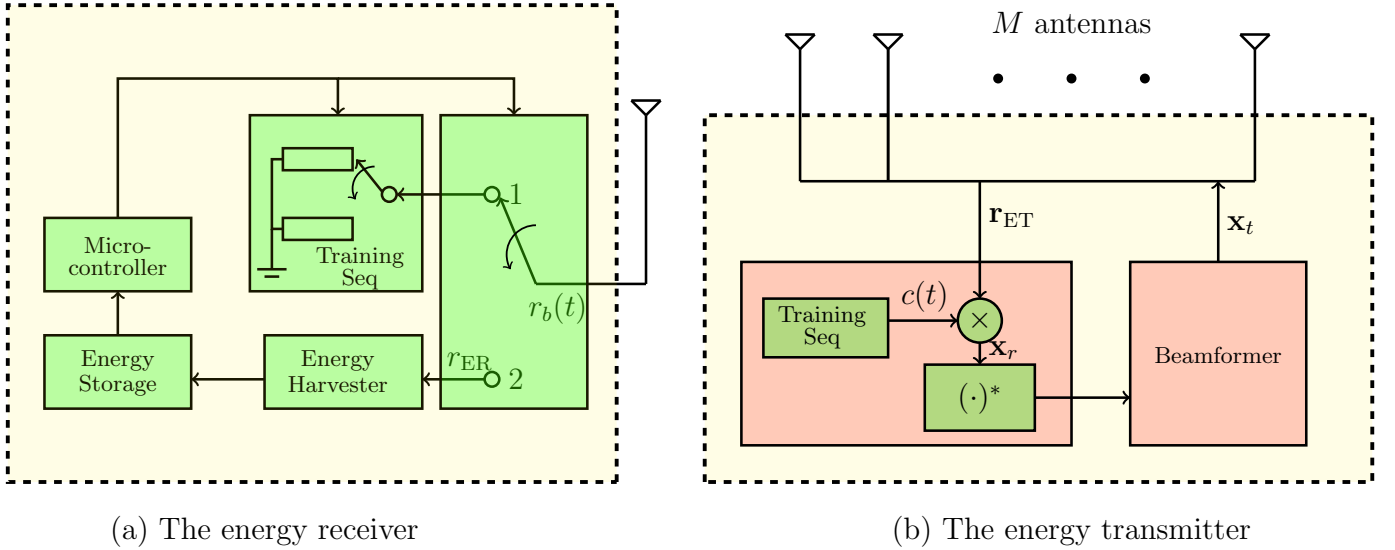


Fig. 2: Block diagram of the energy transmitter and receiver.

training signal composed of a sequence of $+1$ and -1 pulses governed by the backscatter coefficient. This training sequence applied at the ER is quite similar to the Direct Sequence Spread Spectrum (DSSS) [39]. Henceforth, we will also refer to the short duration pulses of switching the reflection coefficient as ‘chips’ and T_c as the chip duration due to the similarity of this scenario with DSSS.

The ET receives the composite signal consisting of the backscattered signal from the ER as well as the ambient signal and noise. The ET correlates this composite signal with the known training sequence $c(t)$. In this work, we assume perfect timing synchronization at the ET, in the baseline case. We then investigate the impact of imperfect synchronization in Section VI.

The purpose of using backscatter training is as follows. In general, the ambient signal is much stronger than the backscattered signal. This is because the latter suffers pathloss and attenuation twice and is orders of magnitude smaller than the former. The training performed at the ER before backscattering opens up a possibility for dealing with this issue of direct-link interference from the ambient signal at the ET. This is discussed in Section V.

2) *The Power Transfer Phase:* During the power transfer phase, the ET provides wireless power transfer to the ER by retrodirective beamforming. Specifically, the ET conjugates the phase of the de-spread signal and each antenna at the ET sends a single-tone sinusoidal waveform towards the ER as shown in Fig. 2b. The phase and amplitude of this waveform are set according to the conjugated signal produced by the

retrodirective antenna, subject to the maximum total transmit power P_t at the ET. The switch in the ER in Fig. 2a moves to position 2. Consequently, the ER stops backscattering and only harvests energy from the energy beam directed to it by the ET, where ζ denote the energy harvesting efficiency. This energy is stored in the energy storage device in the ER.

III. SIGNAL MODEL

In this section, we present the signal equations that form the basis of analysis and design in the later sections. We adopt a continuous-time baseband signal model.

A. The Ambient Signal

For simplicity, similar to the previous works [38], we model the ambient signal as

$$s(t) = \sqrt{P_s} \sum_{i=1}^{\infty} s_i p_s(t - iT_s), \quad (1)$$

where $s_i \sim \mathcal{CN}(0, 1)$ and $p_s(t)$ is a rectangular pulse of duration T_s given by

$$p_s(t) = \begin{cases} 1, & 0 \leq t \leq T_s \\ 0, & t > T_s. \end{cases} \quad (2)$$

Note that the power of an ambient symbol in (1) is P_s .

B. The Backscatter Phase

In the backscatter phase, as described in Section II, the backscattered signal from the ER is given by

$$r_b(t) = \sqrt{\gamma_1} g c(t) s(t), \quad (3)$$

where $c(t)$ is the training sequence with length N_c and chip duration T_c . It can be modelled as

$$c(t) = \sum_{n=0}^{N_c-1} c_n p_c(t - nT_c), \quad (4)$$

where c_n is the n -th chip (+1 or -1) of the training sequence and $p_c(t)$ is a rectangular pulse of duration T_c , i.e.,

$$p_c(t) = \begin{cases} 1, & 0 \leq t \leq T_c \\ 0, & t > T_c. \end{cases} \quad (5)$$

The received signal at the ET is given by

$$\begin{aligned}\mathbf{r}_{\text{ET}}(t) &= \sqrt{\gamma_2}\mathbf{f}r_b(t) + \sqrt{\gamma_3}\mathbf{h}s(t) + \mathbf{n}(t) \\ &= \sqrt{\gamma_1\gamma_2}g\mathbf{f}c(t)s(t) + \sqrt{\gamma_3}\mathbf{h}s(t) + \mathbf{n}(t),\end{aligned}\quad (6)$$

where $\mathbf{n}(t) \sim \mathcal{CN}(0, \sigma_n^2 \mathbf{I}_M)$ is the AWGN. Note that $\mathbf{r}_{\text{ET}}(t)$ is a composite signal with three components, i.e., the backscattered signal from the ER, the ambient signal from the AS and the AWGN. The ET correlates this composite signal with the known training sequence with perfect frame synchronization to give

$$\begin{aligned}\mathbf{x}_r &= \frac{1}{N_c T_c} \int_0^{N_c T_c} \mathbf{r}_{\text{ET}}(t) c(t) dt \\ &= \underbrace{\frac{1}{N_c T_c} \int_0^{N_c T_c} \sqrt{\gamma_1\gamma_2}g\mathbf{f}c(t)s(t)c(t) dt}_{\mathbf{x}_s} + \underbrace{\frac{1}{N_c T_c} \int_0^{N_c T_c} \sqrt{\gamma_3}\mathbf{h}s(t)c(t) dt}_{\mathbf{x}_i} + \underbrace{\frac{1}{N_c T_c} \int_0^{N_c T_c} \mathbf{n}(t)c(t) dt}_{\tilde{\mathbf{n}}},\end{aligned}\quad (7)$$

where \mathbf{x}_s and \mathbf{x}_i are desired signal and undesired ambient (i.e., interference) components at the output of the correlator. Substituting the value of $c(t)$ from (4), we get \mathbf{x}_s and \mathbf{x}_i as

$$\begin{aligned}\mathbf{x}_s &= \frac{\sqrt{\gamma_1\gamma_2}g\mathbf{f}}{N_c T_c} \int_0^{N_c T_c} s(t) \sum_{n=0}^{N_c-1} c_n p_c(t - nT_c) \sum_{m=0}^{N_c-1} c_m p_c(t - mT_c) dt, \\ &= \frac{\sqrt{\gamma_1\gamma_2}g\mathbf{f}}{N_c T_c} \int_0^{N_c T_c} \sum_{n=0}^{N_c-1} c_n^2 s(t) p_c^2(t - nT_c) dt.\end{aligned}\quad (8)$$

$$\begin{aligned}\mathbf{x}_i &= \frac{1}{N_c T_c} \int_0^{N_c T_c} \sqrt{\gamma_3}s(t)c(t)\mathbf{h} dt, \\ &= \frac{\sqrt{\gamma_3}\mathbf{h}}{N_c T_c} \int_0^{N_c T_c} s(t) \sum_{n=0}^{N_c-1} c_n p_c(t - nT_c) dt.\end{aligned}\quad (9)$$

C. Power Transfer Phase

Once the received signal is correlated with the local copy of the training sequence, the large retrodirective antenna array conjugates the phase of the signal at the output of the correlator in (7) and hence beamforms towards the ER. Thus, the signal transmitted by the ET is a single-tone sinusoidal waveform subject to the maximum total transmit power P_t at the ET. It is given as,

$$\mathbf{x}_t = \sqrt{P_t} \frac{(\mathbf{x}_r)^*}{\|\mathbf{x}_r\|}, \quad (10)$$

where $\|\mathbf{x}_r\| = \sqrt{\mathbf{x}_r^T \mathbf{x}_r}$. Note that in (10), we have dropped the time index t because the baseband signal x_t does not vary with time. The signal received by the ER in the power transfer phase is given by

$$\begin{aligned} r_{\text{ER}} &= \sqrt{\gamma_2} \mathbf{f}^T \mathbf{x}_t, \\ &= \sqrt{\gamma_2 P_t} \frac{(\mathbf{f}^T \mathbf{x}_s^* + \mathbf{f}^T \mathbf{x}_i^* + \mathbf{f}^T \tilde{\mathbf{n}}^*)}{\|\mathbf{x}_s + \mathbf{x}_i + \tilde{\mathbf{n}}\|}, \end{aligned} \quad (11)$$

where \mathbf{x}_s is given in (8), \mathbf{x}_i is given in (9) and $\tilde{\mathbf{n}} \sim \mathcal{CN}(0, \frac{\sigma_n^2}{N_c T_c} \mathbf{I}_M)$ is the noise at the output of the matched filter. Note that the receiver noise at the ER is not included in (11) because it is irrelevant to energy harvesting.

D. Metric

In this work, we use the average harvested power at the ER, \overline{Q} , as the figure of merit. It is defined as

$$\overline{Q} = E[Q] = E[\zeta |r_{\text{ER}}|^2], \quad (12)$$

where Q is the instantaneous harvested power², r_{ER} is the received signal at the ER during power transfer phase as given in (11) and ζ is the RF-to-DC current energy conversion efficiency.

IV. ANALYSIS OF ENERGY HARVESTED WITH A PN SEQUENCE

In this section, we discuss the ambient backscatter training performed at the ER. As explained before, the ET receives a backscattered ambient signal from the ER. In addition to this, the ET also receives the original ambient signal which is orders of magnitude stronger than its backscattered version from the ER. This is due to the fact that the backscatter signal suffers attenuation twice, i.e., in going from AS to ER and then from ER to ET. As a result, it is considerably weakened and the signal received at the ET during the backscatter phase is predominantly composed of the ambient component.

This problem of recovering the weak backscatter signal in the presence of a much stronger unwanted ambient signal is quite similar to the signal recovery problem in the direct sequence spread spectrum (DSSS). Taking inspiration from that, we consider a pseudo-noise (PN) training sequence at the ER when backscattering, i.e., the backscatter coefficient is switched between $+1$ and -1 in a pseudo-random fashion.

²In this work, we assume unit time in the power transfer phase. Hence, we use the terms energy and power interchangeably.

By doing this, we expect to capitalize on the spreading gain and boost the backscatter signal against the direct-link ambient interference. In order to assess this technique and the impact of the spreading gain, we evaluate the power harvested at the ER during the power transfer phase of this scheme. We assume that the number of ambient symbols in the backscatter phase is N_s , i.e., $T_b = N_s T_s = N_c T_c$.

We analyze the expressions for the desired signal component and the undesired ambient component to find the energy harvested by the ER in the following two cases: (i) $N_s \leq N_c$ and (ii) $N_s \geq N_c$. The main result is presented in the proposition below.

Proposition 1: For the system model considered in Section II, the instantaneous harvested power Q at the ER at the end of the power transfer phase, when the number of antennas at the ET $M \rightarrow \infty$, is given by

$$Q = \begin{cases} \zeta \gamma_2 P_t \left(\frac{\gamma_1 \gamma_2 |g|^2 \mu (M+1) + \gamma_3 \nu \left(\frac{N_s}{N_c} \right)^2 + \frac{\sigma_n^2 N_s}{T_s P_s}}{\gamma_1 \gamma_2 |g|^2 \mu + \gamma_3 \nu \left(\frac{N_s}{N_c} \right)^2 + \frac{\sigma_n^2 N_s}{T_s P_s}} \right) & \text{if } N_s \leq N_c \\ \zeta \gamma_2 P_t \left(\frac{\gamma_1 \gamma_2 |g|^2 \mu (M+1) + \gamma_3 \nu + \frac{\sigma_n^2 N_s}{T_s P_s}}{\gamma_1 \gamma_2 |g|^2 \mu + \gamma_3 \nu + \frac{\sigma_n^2 N_s}{T_s P_s}} \right) & \text{if } N_s \geq N_c \end{cases} \quad (13)$$

where

$$\mu = \left| \sum_{i=1}^{N_s} s_i \right|^2 = \left| \sum_{i=1}^{N_s} s_i^* \right|^2, \quad (14)$$

$$\nu = \left| \sum_{i=1}^{N_s} \sum_{n=\frac{N_c}{N_s}(i-1)}^{\frac{N_c}{N_s}i-1} c_n s_i^* \right|^2 = \left| \sum_{i=1}^{N_s} \sum_{n=\frac{N_c}{N_s}(i-1)}^{\frac{N_c}{N_s}i-1} c_n s_i \right|^2, \quad (15)$$

for simplicity.

Proof: See Appendix A. ■

The general expression obtained for instantaneous harvested power in (13) has two mutually dependent random variables μ and ν , in addition to g , \mathbf{f} and \mathbf{h} . Therefore, it is not possible to obtain a closed form expression for the expected value of harvested power. However, we found the average harvested power by simulation and confirmed the result by numerically taking the average of the expression in (13).

Fig. 3 plots the average harvested power versus the duration of the backscatter phase, i.e., T_b with the ambient signal duration being $T_s = 5 \mu\text{s}$. The remaining values of the system parameters are set as

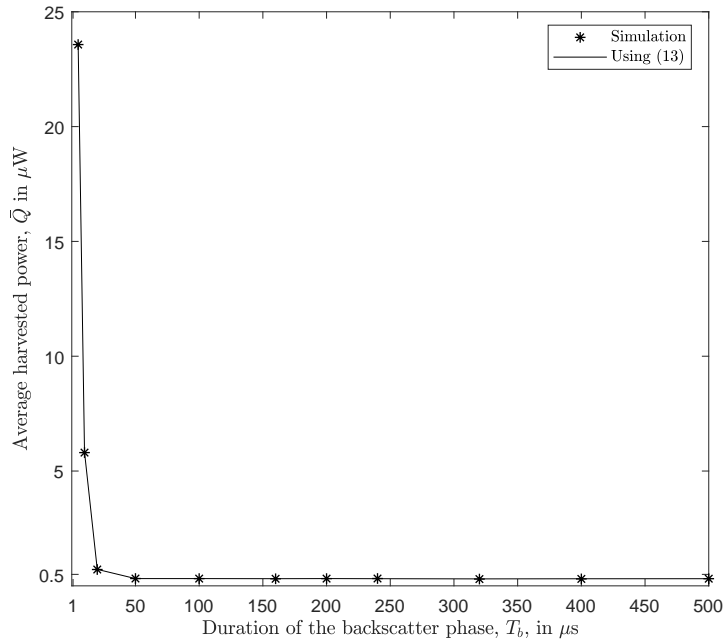


Fig. 3: Average harvested power at the ER as a function of T_b (duration of the backscatter phase).

follows: $d_1 = 10$ m, $d_2 = 20$ m, $d_3 = 18$ m, $d_0 = 1$ m, $k_0 = 0.001$, $M = 500$, $P_t = 1$ W, $P_s = 1$ W, $\sigma_n^2 = 10^{-18}$, $\zeta = 0.5$, $T_c = 500$ ns. The choice of $T_c = 500$ ns ensures that multipath delay spread is negligible [34]. The results in Fig. 3 are averaged over 10^4 Monte Carlo simulation trials. In each trial, a new pseudorandom sequence is generated and used. Note that for other practical values of system parameters, the average harvested power has very similar values and trend. Thus, we only show a single curve in Fig. 3.

The figure shows that there is a very good agreement between the analytical results in (13) and the simulation for $N_s \leq N_c^3$. The figure also shows that the average harvested power is maximum around $24 \mu\text{W}$ when $N_s = 1$ and $T_b = 5 \mu\text{s}$. As N_s and hence T_b increase, the average harvested power quickly decreases and reaches a value of approximately $0.3 \mu\text{W}$. Thus, two main observations can be made from the plot. Firstly, the average harvested power is very small. Secondly, the harvested power reduces further as the training period increases.

This second observation is particularly counter-intuitive, since it is not expected to happen when using

³A similar match is observed between the analytical result and the simulation for $N_s \geq N_c$ but the corresponding plots are not presented here due to the reason discussed in Remark 1 on the next page.

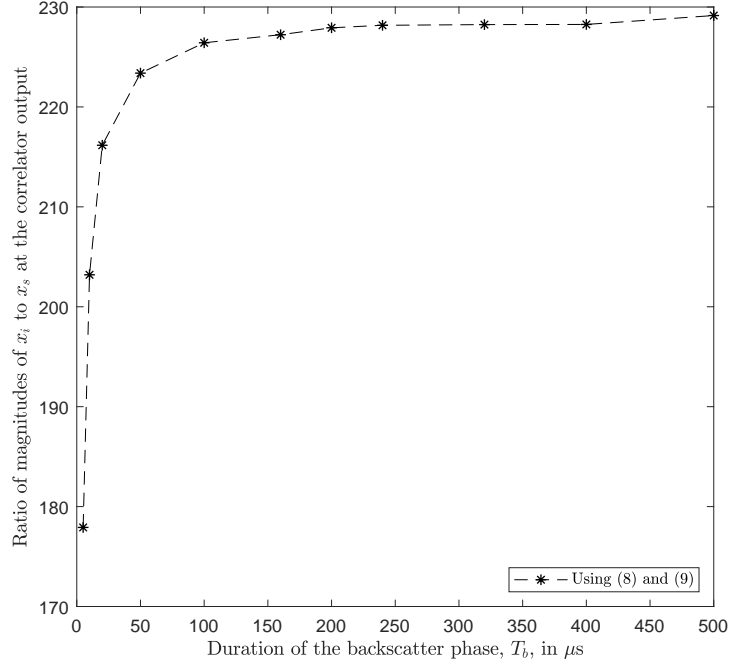


Fig. 4: Ratio of magnitude of ambient and backscatter signal components at the output of the correlator plotted against T_b (duration of the backscatter phase).

DSSS techniques. The reason for this trend is that the ambient signal is orders of magnitude stronger than the backscattered signal. The spreading gain of the training sequence employed is not sufficient to boost the backscatter signal significantly against the ambient signal. In order to demonstrate this, Fig. 4 plots $\frac{|x_i|}{|x_s|}$, i.e., the ratio of the magnitudes of the undesired ambient component and the desired backscatter component at the output of the correlator versus the duration of the backscatter phase T_b . We can see from the figure that even with the training sequence in use, the ambient component is much stronger than the desired backscattered signal. Moreover, as the duration of the training phase increases, the ambient component becomes increasingly stronger. Thus, when the ET performs retrodirective beamforming in the power transfer phase by taking the conjugate of the composite signal at the output of the correlator, the comparative strength of the ambient component is far greater than the backscattered one for large durations of backscatter phase. Thus, most of the energy transmitted by the ET is still effectively leaking towards the AS and this situation becomes exacerbated for longer durations of backscatter phase due to the comparatively higher strength of the ambient component.

Remark 1: We have presented the average harvested power for the two possible cases of $N_s \leq N_c$ and $N_s \geq N_c$ in (13). However, we can see from Fig. 3 that the harvested power becomes very low with increasing values of N_s . As N_s exceeds N_c , the average harvested power stays perpetually low, in fractions of μs . This is due to the fact that the proposed scheme depends upon the variation of the backscatter coefficient during each ambient symbol that is backscattered. Consequently, we have presented the results for $N_s \leq N_c$ only in Fig. 3. Moreover, since the PN-sequence approach for training design fails to boost up the backscattered signal in the presence of the strong ambient interference, another approach of training sequence design is considered in the next section, that directly looks at eliminating the ambient interference. This new scheme relies on the variation of the backscatter coefficient between ± 1 during each ambient symbol. Therefore, from this point onwards, we only consider the case $N_s \leq N_c$.

V. THE PROPOSED TRAINING SEQUENCE DESIGN

As mentioned in the previous section, the purpose of employing backscatter training was to enable the ET to differentiate the backscattered transmission from the ambient signal. However, since the backscattered signal is orders of magnitude weaker than the ambient interference and the DSSS approach cannot boost up the backscatter signal, the only option left is to directly cancel or significantly suppress the ambient interference. In the following, we propose a scheme to remove the direct-link interference from the AS.

Design Criterion: For the system model considered in Section II, the ambient component can be eliminated at the output of the correlator in the ET if for each ambient symbol that is backscattered from the ER during the backscatter phase, the number of $+1$ and -1 chips is equal, i.e., $N_{+1} = N_{-1}$ and $N_{+1} + N_{-1} = \frac{N_c}{N_s}$, where N_{+1} and N_{-1} are the number of positive and negative chips respectively that are multiplied per symbol of the ambient source. This means that the backscatter coefficient is switched between $+1$ and -1 an even number of times, i.e., $N_c = 2kN_s$ where k is a positive integer.

We justify the above design criterion as follows: In this case, $c(t)$ is a deterministic sequence of equal number of $+1$ and -1 chips instead of a PN sequence. Any sequence with equal number of $+1$ and -1 chips applied to each ambient symbol while backscattering, does the job. So we consider the expressions

for \mathbf{x}_s and \mathbf{x}_i , which are the expanded forms of (8) and (9) for $N_s \leq N_c$, and are given below

$$\mathbf{x}_s = \sqrt{\gamma_1 \gamma_2 P_s} \frac{g \mathbf{f}}{N_s} \sum_{i=1}^{N_s} s_i. \quad (16)$$

$$\mathbf{x}_i = \sqrt{\gamma_3 P_s} \frac{\mathbf{h}}{N_c} \sum_{i=1}^{N_s} s_i \sum_{n=\frac{N_c}{N_s}(i-1)}^{\frac{N_c}{N_s}i-1} c_n. \quad (17)$$

We can see from (16) that, the desired backscattered component at the output of the correlator \mathbf{x}_s does not depend on the attributes of the training sequence, i.e., how the backscatter coefficient is changed. Therefore, it remains the same as in the previous case. However, with our proposed training sequence satisfying the *design criterion*, (17) becomes

$$\begin{aligned} \mathbf{x}_i &= \sqrt{\gamma_3 P_s} \frac{\mathbf{h}}{N_c} \sum_{i=1}^{N_s} s_i \sum_{n=\frac{N_c}{N_s}(i-1)}^{\frac{N_c}{N_s}i-1} c_n, \\ &= \sqrt{\gamma_3 P_s} \frac{\mathbf{h}}{N_c} \sum_{i=1}^{N_s} s_i [(+1)N_{+1} + (-1)N_{-1}] = 0 \end{aligned} \quad (18)$$

since $N_{+1} = N_{-1}$. Thus, the ambient component at the output of the correlator cancels out.

Using the proposed sequence in the *design criterion*, we find the average harvested energy at the ER, which is presented in the proposition below.

Proposition 2: For the system model considered in Section II and employing the backscatter training scheme proposed in the *design criterion*, the instantaneous harvested power at the ER at the end of the power transfer phase when the number of antennas at the ER $M \rightarrow \infty$, is given by

$$Q \approx \zeta \gamma_2 P_t \left(\frac{\gamma_1 \gamma_2 |g|^2 \mu (M+1) + \frac{\sigma_n^2 N_s^2}{N_c T_c P_s}}{\gamma_1 \gamma_2 |g|^2 \mu + \frac{\sigma_n^2 N_s^2}{N_c T_c P_s}} \right). \quad (19)$$

From (19) we can obtain the average harvested power at the ER, given by

$$\bar{Q} \approx \frac{\zeta P_t \sigma_n^2}{T_s P_s \gamma_1} \left((M+1) G_{1 \frac{3}{2}}^{\frac{3}{2} \frac{1}{2}} \left(\frac{-1}{-1, 0, 0} \left| \frac{\sigma_n^2}{P_s T_s \gamma_1 \gamma_2} \right. \right) + G_{1 \frac{3}{2}}^{\frac{3}{2} \frac{1}{2}} \left(\frac{0}{0, 0, 0} \left| \frac{\sigma_n^2}{P_s T_s \gamma_1 \gamma_2} \right. \right) \right), \quad (20)$$

where μ is as defined in (14) and $G_{p \ q}^{m \ n} \left(\begin{smallmatrix} a_1, \dots, a_p \\ b_1, \dots, b_q \end{smallmatrix} \middle| z \right)$ is the MeijerG function [36].

Proof: See Appendix B. ■

Using (20), the average harvested energy at the ER is plotted in Fig. 5 for three different values of ambient symbol duration, i.e., $T_s = 5 \mu\text{s}$, $T_s = 10 \mu\text{s}$ and $T_s = 20 \mu\text{s}$. The values of other system

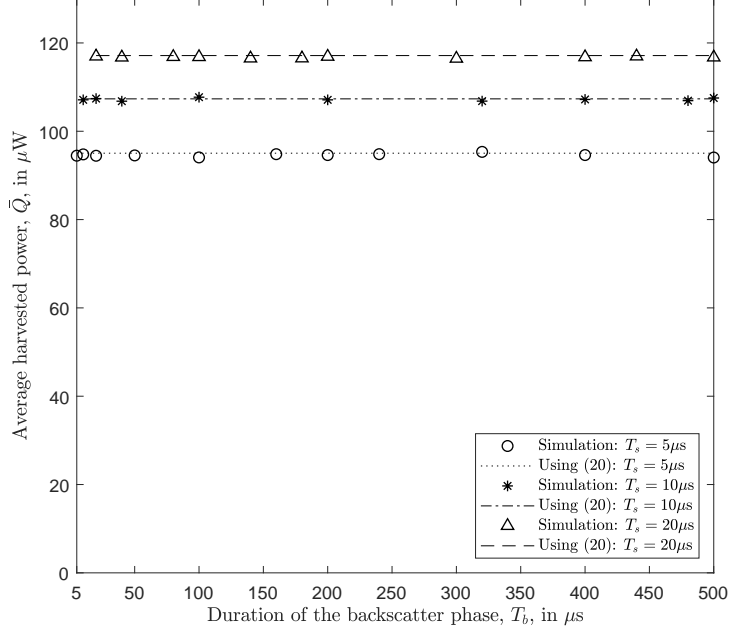


Fig. 5: Average harvested power at the ER with the proposed sequence plotted against the duration of the backscatter phase, T_b .

parameters are the same as stated in Section IV for Fig. 3. Numerous features of this scheme are evident from Fig. 5. Firstly, it can be observed that the energy harvested at the ER increases significantly as compared to the case when a pseudo-random sequence is employed at the ER during the backscatter phase. This is due to the fact that the proposed scheme completely eliminates the ambient component. As a result, the retrodirective beamformer forms a focused beam directed back at the ER alone, with no energy leaking to the AS.

Secondly, the harvested power at the ER does not change with the increase in backscatter training duration, but stays constant as long as the ambient symbol duration T_s stays constant. This is confirmed by the result given in (20) as the average harvested energy is independent of the duration of the backscatter phase T_b . Specifically, when the system is designed with a fixed value of T_c , then for different values of N_s and hence T_b , the average harvested power at the ER now stays at $95 \mu W$ for $T_s = 5 \mu s$, $108.3 \mu W$ for $T_s = 10 \mu s$ and $116.4 \mu W$ for $T_s = 20 \mu s$.

Thirdly, with the ambient component removed, the average harvested power depends largely on the

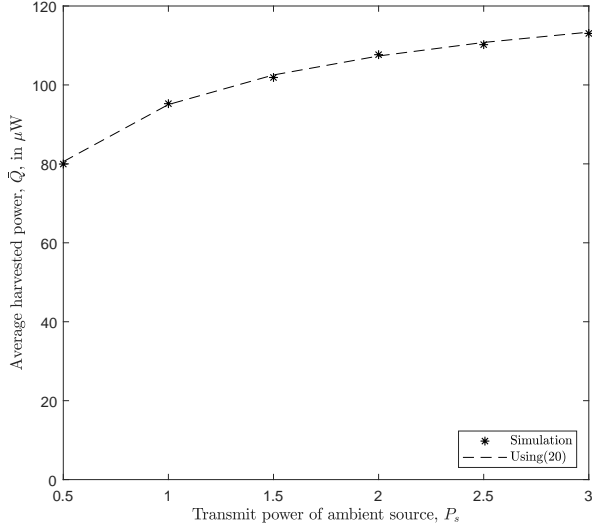


Fig. 6: Average harvested power, \bar{Q} , plotted against transmit power of AS, P_s .

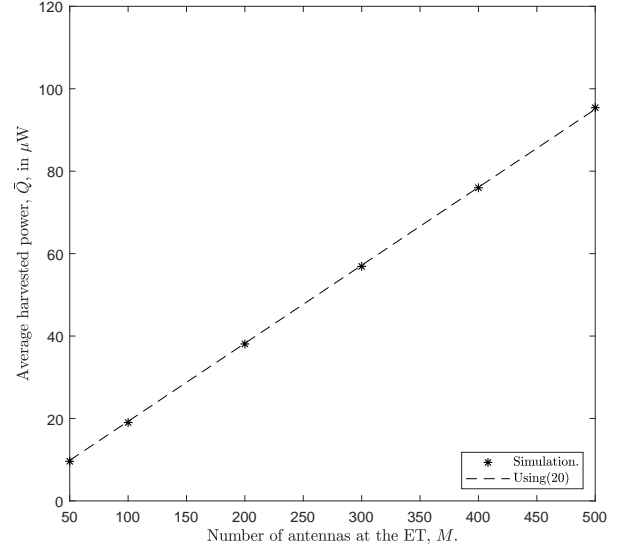


Fig. 7: Average harvested power, \bar{Q} , plotted against number of antennas at the ET M .

duration of the ambient symbol T_s , as is evident from the plot with the average harvested power having a significantly larger value for $T_s = 20 \mu\text{s}$, compared to $T_s = 5 \mu\text{s}$

Lastly, it can also be inferred from the plot that for a fixed ambient source, the average harvested power in this case is independent of the number of chips N_c . Actually, for a fixed chip duration, the number of chips also increases with the increased backscatter period T_b and as we can see from Fig. 5, the average harvested power stays constant for the increased values of the backscatter period.

We can see from (16) that the desired backscatter component \mathbf{x}_s is directly proportional to the strength of the AS. Since the ambient component is now completely removed, a higher value of power is harvested on average at the ER when the AS is stronger. Fig. 6 presents the plots of average harvested power against the duration of backscatter phase T_b for different values of P_s , the power of the AS. We can see that the average harvested power is larger with higher values of P_s . Similarly, Fig. 7 plots the average harvested power against M , the number of antennas at the ET. It can be observed that there is a good agreement again between the results obtained by simulation and by using (20) for practical values of M .

Remark 2: The *design criterion* is generic, i.e., any sequence that satisfies the two properties can serve the purpose. Moreover, we have seen that once the ambient component is removed, having a greater number

of chips does not affect the harvested energy. Therefore, taking into account the hardware implementation, it is best to have the minimum number of chips per ambient symbol period, i.e., $k = 1$ and $N_c = 2N_s$ or $T_c = \frac{T_s}{2}$. This means that we can switch the backscatter coefficient only twice per ambient symbol, i.e., for each ambient symbol that is backscattered, the backscatter coefficient is kept $+1$ for half of the ambient symbol duration and -1 for the other half.

Remark 3: It is interesting to see how this design criterion compares with the well-known training sequences commonly used in wireless communications, i.e., Maximal length sequences, Gold sequences, Walsh-Hadamard sequences and Kasami sequences. Out of these, only the Walsh-Hadamard sequences have equal number of $+1$ and -1 and hence satisfy the *design criterion*.

VI. IMPACT OF PRACTICAL SYSTEM IMPERFECTIONS

In the previous section, we propose a training design and concluded, under the perfect synchronization assumption, that the number of chips (or equivalently the switching rate) does not matter, as long as there are the same number of $+1$ chips and -1 chips over one ambient symbol. However, in practice, if the ambient symbol duration is unknown or changes from the one for which the system is designed, it may lead to the loss of timing synchronization at the correlator in the ET or unequal durations of $+1$ and -1 values of the backscatter coefficient at the ER. Consequently, the ambient signal may not be completely cancelled and the performance of the system in terms of average harvested power at the ER may be affected. In this section, we study the impact of the following two system imperfections caused by the unknown duration of the ambient symbol.

A. Imperfect synchronization at the correlator

The results in the previous sections assume perfect synchronization. In this sub-section, we consider the case when an integer number of ambient symbols fit in the duration of the backscatter phase, but there is a misalignment between the received signal at ET and the locally generated training sequence during the backscatter phase. We model this misalignment as a time offset T_{off} .

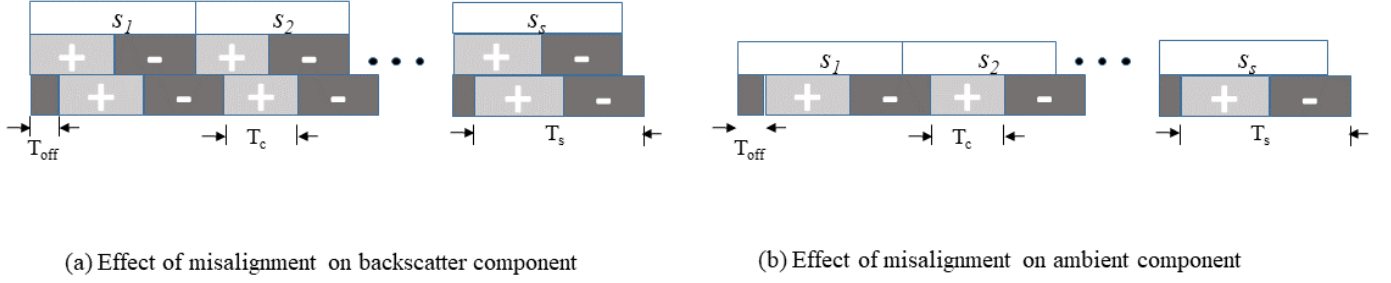


Fig. 8: Misalignment between the backscattered signal and locally generated spreading sequence at the ET.

1) *Effect of offset on the desired signal component:* We assume that the timing offset $T_{\text{off}} < T_c$. This is shown in Fig. 8. In this case, the desired component at the output of the correlator in (8) becomes

$$\begin{aligned}
 \mathbf{x}_s &= \frac{\sqrt{\gamma_2 \gamma_1} g \mathbf{f}}{N_c T_c} \int_0^{N_c T_c} \sum_{n=0}^{N_c-1} s(t) c_n p_c(t - n T_c) \sum_{m=0}^{N_c-1} c_m p_c(t - T_{\text{off}} - m T_c) dt, \\
 &\stackrel{(a)}{=} \sqrt{\gamma_1 \gamma_2} P_s \frac{g \mathbf{f}}{N_c T_c} \sum_{i=1}^{N_s} s_i \frac{N_c}{N_s} \left(\int_0^{T_{\text{off}}} -1 dt + \int_{T_{\text{off}}}^{T_c} 1 dt \right), \\
 &= \sqrt{\gamma_1 \gamma_2} P_s \frac{g \mathbf{f}}{N_c T_c} \sum_{i=1}^{N_s} s_i \frac{N_c}{N_s} (-2 T_{\text{off}} + T_c), \\
 &= \sqrt{\gamma_1 \gamma_2} P_s \frac{g \mathbf{f}}{N_c T_c} \sum_{i=1}^{N_s} s_i \frac{N_c T_c}{N_s} \left(1 - 2 \frac{T_{\text{off}}}{T_c} \right), \\
 &= \sqrt{\gamma_1 \gamma_2} P_s \frac{g \mathbf{f}}{N_s} \sum_{i=1}^{N_s} s_i \left(1 - 2 \frac{T_{\text{off}}}{T_c} \right), \tag{21}
 \end{aligned}$$

where (a) splits the overall integration into intervals over each symbol.

Comparing (8) and (21) above we get for $T_{\text{off}} \leq T_c$

$$\mathbf{x}_{s(\text{misaligned})} = \left(1 - 2 \frac{T_{\text{off}}}{T_c} \right) \mathbf{x}_{s(\text{synchronized})}. \tag{22}$$

Similarly, it can be shown that for $T_c < T_{\text{off}} \leq 2 T_c$,

$$\mathbf{x}_{s(\text{misaligned})} = \left(2 \frac{T_{\text{off}}}{T_c} - 1 \right) \mathbf{x}_{s(\text{synchronized})}. \tag{23}$$

Thus, we can see that if the synchronization is not perfect, the desired backscatter component is a fraction of the fully synchronized case.

2) *Effect of offset on the undesired ambient component:* Again assuming that the timing offset $T_{\text{off}} < T_c$, the undesired ambient component from (9) at the output of the correlator becomes,

$$\begin{aligned}
\mathbf{x}_i &= \frac{\sqrt{\gamma_3} \mathbf{h}}{N_c T_c} \int_0^{N_c T_c} \sum_{m=0}^{N_c-1} c_m p_c(t - T_{\text{off}} - n T_c) s(t) dt, \\
&= \frac{\sqrt{\gamma_3} \mathbf{h}}{N_c T_c} \int_0^{N_c T_c} \sum_{m=0}^{N_c-1} c_m p_c(t - T_{\text{off}} - n T_c) \sqrt{P_s} \sum_{i=1}^S s_i P_s(t - i T_s) dt, \\
&= \sqrt{\gamma_3 P_s} \frac{\mathbf{h}}{N_c T_c} \sum_{i=1}^{N_s} s_i \left(\int_0^{T_{\text{off}}} -1 dt + \int_{T_{\text{off}}}^{T_c} +1 dt + \int_{T_c}^{2T_c} -1 dt + \cdots + \int_{(\frac{N_c}{N_s}-1)T_c}^{\frac{N_c}{N_s}T_c - T_{\text{off}}} -1 dt \right), \\
&= \sqrt{\gamma_3 P_s} \frac{\mathbf{h}}{N_c T_c} \sum_{i=1}^{N_s} s_i (-T_{\text{off}} + T_c - T_c + T_c \cdots - T_c + T_{\text{off}}), \\
&= 0.
\end{aligned} \tag{24}$$

The same result is obtained even when $T_{\text{off}} > T_c$. As we have seen in the previous sub-section, the desired component is scaled down because of the offset in synchronization while the undesired component is still completely being eliminated. This change in the magnitude of the desired component is reflected in the energy harvested at the ER. *Therefore, we can conclude that the system can work reasonably well with a small timing offset. However good synchronization is needed for best performance.*

Using the above values of \mathbf{x}_s and \mathbf{x}_i , the average harvested energy at the ER in case of misalignment at the ET can be shown to be given by

$$\bar{Q} \approx \frac{\zeta P_t \sigma_n^2}{P_s T_s \gamma_1} \left((M+1) G_{1 \ 3}^3 \left(\begin{matrix} -1 \\ -1, 0, 0 \end{matrix} \middle| \frac{\sigma_n^2}{P_s T_s \gamma_1 \gamma_2 \left| 1 - \frac{2T_{\text{off}}}{T_c} \right|} \right) + G_{1 \ 3}^3 \left(\begin{matrix} 0 \\ 0, 0, 0 \end{matrix} \middle| \frac{\sigma_n^2}{P_s T_s \gamma_1 \gamma_2 \left| 1 - \frac{2T_{\text{off}}}{T_c} \right|} \right) \right). \tag{25}$$

which holds for all values of T_{off} except when $T_{\text{off}} = k \frac{T_c}{2}$ where k is a an integer and $k \geq 0$. A plot of the average harvested power at the ER as a function of time offset between the received and locally generated signal is given in Fig. 9. The parameter values used are the same as for Fig. 5. For this plot we have taken $T_c = \frac{T_s}{2}$, as discussed in Remark 2 in Section V. It can be seen from Fig. 9 that the average harvested power decreases for $kT_c \leq T_{\text{off}} < k \frac{T_c}{2}$, becoming zero at $T_{\text{off}} = k \frac{T_c}{2}$ and then increases for $k \frac{T_c}{2} < T_{\text{off}} \leq kT_c$.

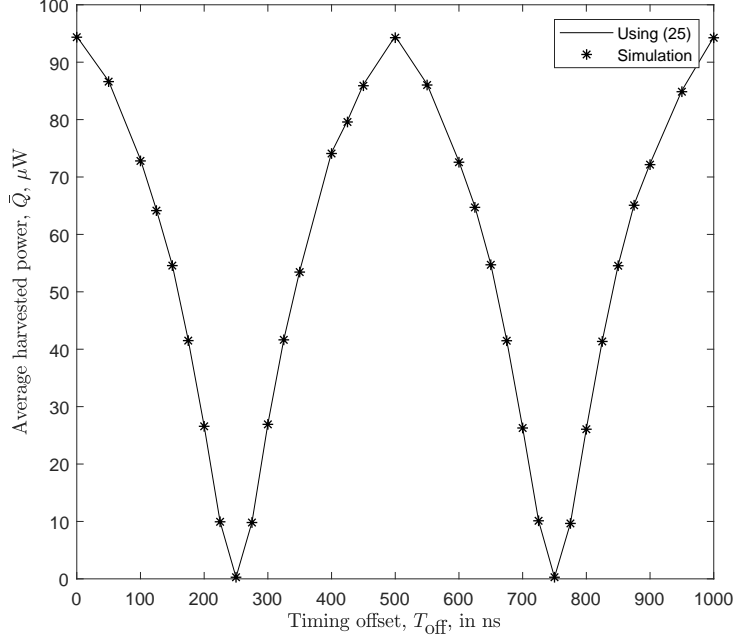


Fig. 9: Average harvested power at the ER plotted against the offset between incoming and locally generated signal at the correlator.

B. Effect of change in ambient symbol duration

In this subsection, we consider the case where due to unknown ambient symbol duration, an even number of chips or backscatter coefficient changes do not fit in each ambient symbol. Consider the scenario in which the system is designed for an ambient symbol duration T_s . However, when the system is actually deployed, the available ambient symbol has a different duration, i.e., T'_s . In this situation, the energy transfer performance under the proposed training scheme with $\frac{N_c}{N_s} = 2$ is expected to be severely degraded.

We demonstrate this fact by means of simulation results. Fig. 10 plots the average harvested power at the ER versus the number of ambient symbols that fit in the backscatter phase duration of T_b seconds for training sequences that satisfy the *design criterion* but have different number of chips, i.e., $\frac{N_c}{N_s} = 2, 10$ and 40. This system was originally designed for the following values: $T_b = 200 \mu\text{s}$, $N_c = 400$, $T_c = 500 \text{ ns}$, $T_s = 20 \mu\text{s}$, $N_s = 10$. We plot the average harvested power at the ER for a range of values of $N'_s = \{6, 7, 8, 9, 10, 11, 12, 13, 14, 15\}$ and the corresponding T'_s .

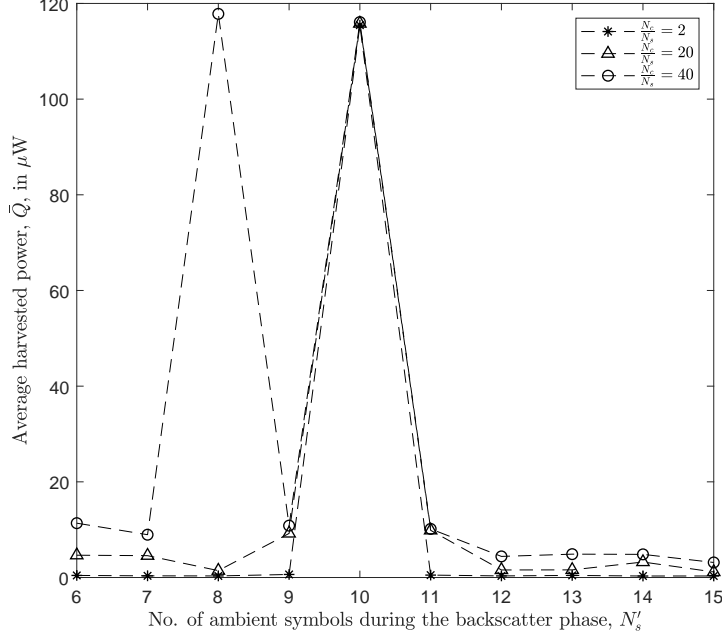


Fig. 10: Average harvested power at the ER plotted against the number of ambient symbols during the backscatter phase when the actual ambient symbol duration is different from the designed value.

We can see from Fig. 10 that the training sequence with the least number of chips per symbol gives the worst performance, i.e., as the number of the ambient symbols in the backscatter phase deviates from designed value, the average harvested power drops to a fraction of a μW . This is due to the fact that the ambient component is no longer completely cancelled as the ER was designed to switch the backscatter coefficient at $\frac{T_s}{2}$, so that each ambient symbol was multiplied by $+1$ and -1 for alternate halves of its duration. However, in the new scenario, a switch at $\frac{T'_s}{2}$ is required. Consequently, the ambient component is not eliminated completely; rather a fraction from each ambient symbol remains that contributes to a residual ambient component at the output of the correlator. This, in turn leads to a significant amount of power leaking to the AS.

It can also be observed from Fig. 10 that as the number of chips per ambient symbol increase, better performance can be obtained. For instance, the curve with the largest number of chips per symbol, i.e., $\frac{N_c}{N_s} = 40$ performs relatively better than the other two cases for moderate mismatch in symbol duration. The reason for this behaviour is that the fraction of ambient component that is not cancelled due to the

unknown value of T_s depends upon the chip duration T_c . Therefore, in spite of the fact that an even number of chips may not fit in one ambient symbol, leading to imperfect cancellation, by increasing the switching rate of the backscatter coefficient and thereby decreasing the chip duration T_c , the un-cancelled fraction of a chip can be reduced and hence a smaller ambient component remains at the output of the correlator. Hence, there is less leakage towards the AS and the ER is able to harvest more power. Thus, when the ambient symbol duration is unknown, a faster switching rate can help to minimize the effect of uncanceled ambient for moderate mismatch of symbol duration.

VII. CONCLUSIONS AND FUTURE WORK

In this work we have presented a wireless power transfer scheme to energize an ER using retrodirective beamforming at the ET and ambient backscatter at the ER. To deal with the direct-link ambient interference, we proposed the approach of backscatter training, i.e., the pattern of varying the reflection coefficient at the ER to completely eliminate the strong direct-link ambient interference. We showed that when the ambient symbol duration is known, the switching rate does not matter and we can switch the backscatter coefficient only twice per ambient symbol period. When the ambient symbol duration is unknown, then switching at a faster rate helps to minimize the effect of the uncanceled ambient and boost the harvested power. In this paper, we have dealt with the baseline case of WPT between one ET and one ER. Future work can consider the case of multiple ETs and ERs taking scheduling and collision resolution into account.

APPENDIX A

PROOF OF PROPOSITION 1

We derive the formula for instantaneous energy harvested at the ER during the power transfer phase as given in (13). We consider the following two cases:

Case 1: $N_s \leq N_c$ In this case, we have $T_s \geq T_c$. Substituting (1) in (8) we have

$$\mathbf{x}_s = \frac{\sqrt{\gamma_1 \gamma_2} g \mathbf{f}}{N_c T_c} \int_0^{N_c T_c} \sum_{n=0}^{N_c-1} c_n^2 p_c^2(t - nT_c) \sqrt{P_s} \sum_{i=1}^{N_s} s_i p_s(t - iT_s) dt, \quad (26a)$$

$$= \frac{\sqrt{\gamma_1 \gamma_2} \overline{P_s} g \mathbf{f}}{N_c T_c} \sum_{i=1}^{N_s} s_i \sum_{n=\frac{N_c}{N_s}(i-1)}^{\frac{N_c}{N_s}i-1} c_n^2 \int_{nT_c}^{(n+1)T_c} p_c^2(t - nT_c) dt, \quad (26b)$$

$$= \sqrt{\gamma_1 \gamma_2} \overline{P_s} \frac{g \mathbf{f}}{N_c T_c} \sum_{i=1}^{N_s} \sum_{n=\frac{N_c}{N_s}(i-1)+1}^{\frac{N_c}{N_s}i} c_n^2 s_i T_c, \quad (26c)$$

$$= \sqrt{\gamma_1 \gamma_2} \overline{P_s} \frac{g \mathbf{f}}{N_c} \frac{N_c}{N_s} \sum_{i=1}^{N_s} s_i, \quad (26d)$$

$$= \sqrt{\gamma_1 \gamma_2} \overline{P_s} \frac{g \mathbf{f}}{N_s} \sum_{i=1}^{N_s} s_i, \quad (26e)$$

where the integration in (26b) comes from the fact that the integration in (26a) is being performed for the product of two aligned rectangular pulses $p_c(t)$ and $p_s(t)$ where $T_s \geq T_c$ and the duration of integration is $N_c T_c$. Also, (26d) follows from the fact that $c_n^2 = 1$ and $\sum_{n=\frac{N_c}{N_s}(i-1)}^{\frac{N_c}{N_s}i-1} = \frac{N_c}{N_s}$ for any given i .

Next, substituting (1) in (9) we get

$$\mathbf{x}_i = \frac{\sqrt{\gamma_3} \mathbf{h}}{N_c T_c} \int_0^{N_c T_c} \sqrt{P_s} \sum_{i=1}^{N_s} s_i p_s(t - iT_s) \sum_{n=1}^{N_c} c_n p_c(t - nT_c) dt, \quad (27a)$$

$$= \sqrt{\gamma_3} \overline{P_s} \frac{\mathbf{h}}{N_c T_c} \sum_{i=1}^{N_s} s_i \sum_{n=\frac{N_c}{N_s}(i-1)}^{\frac{N_c}{N_s}i-1} c_n \int_{nT_c}^{(n+1)T_c} p_c(t - nT_c) dt, \quad (27b)$$

$$= \sqrt{\gamma_3} \overline{P_s} \frac{\mathbf{h}}{N_c T_c} \sum_{i=1}^{N_s} \sum_{n=\frac{N_c}{N_s}(i-1)}^{\frac{N_c}{N_s}i-1} c_n s_i T_c, \quad (27c)$$

$$= \sqrt{\gamma_3} \overline{P_s} \frac{\mathbf{h}}{N_c} \sum_{i=1}^{N_s} \sum_{n=\frac{N_c}{N_s}(i-1)}^{\frac{N_c}{N_s}i-1} c_n s_i, \quad (27d)$$

where again the integration in (27a) becomes the summation in (27c) as mentioned above. Substituting (26e) and (27d) into (11), we get

$$r_{\text{ER}} = \sqrt{\gamma_2} \overline{P_t} \frac{\left(\frac{\sqrt{\gamma_1 \gamma_2} \overline{P_s} g^*}{N_s} \sum_{i=1}^{N_s} s_i^* \mathbf{f}^T \mathbf{f}^* + \frac{\sqrt{\gamma_3} \overline{P_s}}{N_c} \sum_{i=1}^{N_s} \sum_{n=\frac{N_c}{N_s}(i-1)+1}^{\frac{N_c}{N_s}i} c_n s_i^* \mathbf{f}^T \mathbf{h}^* + \mathbf{f}^T \mathbf{n}^* \right)}{\left\| \frac{\sqrt{\gamma_1 \gamma_2} \overline{P_s} g^*}{N_s} \sum_{i=1}^{N_s} s_i \mathbf{f} + \frac{\sqrt{\gamma_3} \overline{P_s}}{N_c} \sum_{i=1}^{N_s} \sum_{n=\frac{N_c}{N_s}(i-1)+1}^{\frac{N_c}{N_s}i} c_n s_i \mathbf{h} + \mathbf{n} \right\|}. \quad (28)$$

Since $\mathbf{f}^T \mathbf{f}^* = \mathbf{f}^H \mathbf{f}$ and $\mathbf{f}^T \mathbf{h}^* = \mathbf{f}^H \mathbf{h}$, (28) simplifies to

$$r_{\text{ER}} = \sqrt{\gamma_2 P_t} \frac{(\frac{\sqrt{\gamma_1 \gamma_2 P_s g}}{N_s} \sum_{i=1}^{N_s} s_i^* \mathbf{f}^H \mathbf{f} + \frac{\sqrt{\gamma_3 P_s}}{N_c} \sum_{i=1}^{N_s} \sum_{n=\frac{N_c}{N_s}(i-1)+1}^{\frac{N_c}{N_s} i} c_n s_i^* \mathbf{f}^H \mathbf{h} + \mathbf{f}^H \mathbf{n})}{\left\| \frac{\sqrt{\gamma_1 \gamma_2 P_s g}}{N_s} \sum_{i=1}^{N_s} s_i \mathbf{f} + \frac{\sqrt{\gamma_3 P_s}}{N_c} \sum_{i=1}^{N_s} \sum_{n=\frac{N_c}{N_s}(i-1)+1}^{\frac{N_c}{N_s} i} c_n s_i \mathbf{h} + \mathbf{n} \right\|}. \quad (29)$$

Substituting (29) in (12), we get

$$Q = \zeta |r_{\text{ER}}|^2 = \zeta \left(\frac{\frac{\gamma_1 \gamma_2^2 P_s P_t |g|^2}{N_s^2} \left| \sum_{i=1}^{N_s} s_i \right|^2 \|\mathbf{f}\|^4 + \frac{\gamma_3 P_s P_t}{N_c^2} \left| \sum_{i=1}^{N_s} \sum_{n=\frac{N_c}{N_s}(i-1)+1}^{\frac{N_c}{N_s} i} c_n s_i \right|^2 \|\mathbf{f}^H \mathbf{h}\|^2 + \gamma_2 P_t \|\mathbf{f}^H \mathbf{n}\|^2}{\frac{\gamma_1 \gamma_2 P_s |g|^2}{N_s^2} \left| \sum_{i=1}^{N_s} s_i^* \right|^2 \|\mathbf{f}\|^2 + \frac{\gamma_3 P_s}{N_c^2} \left| \sum_{i=1}^{N_s} \sum_{n=\frac{N_c}{N_s}(i-1)+1}^{\frac{N_c}{N_s} i} c_n s_i^* \right|^2 \|\mathbf{h}\|^2 + \|\mathbf{n}\|^2} \right). \quad (30)$$

Let

$$\begin{aligned} \mu &= \left| \sum_{i=1}^{N_s} s_i \right|^2 = \left| \sum_{i=1}^{N_s} s_i^* \right|^2, \\ \nu &= \left| \sum_{i=1}^{N_s} \sum_{n=\frac{N_c}{N_s}(i-1)+1}^{\frac{N_c}{N_s} i} c_n s_i^* \right|^2 = \left| \sum_{i=1}^{N_s} \sum_{n=\frac{N_c}{N_s}(i-1)+1}^{\frac{N_c}{N_s} i} c_n s_i \right|^2. \end{aligned} \quad (31)$$

Also using the asymptotic massive MIMO expressions [40], i.e. $\frac{1}{M} \|\mathbf{f}_i\|^4 \rightarrow M+1$, $\frac{1}{M} \|\mathbf{f}_i\|^2 \rightarrow 1$, $\frac{1}{M} \|\mathbf{f}_k^H \mathbf{f}_i\|^2 \rightarrow 1$, $\frac{1}{M} \mathbf{f}_k^H \mathbf{f}_i \rightarrow 0$ (for $k \neq i$), $\frac{1}{M} \mathbf{f}_k^H \tilde{\mathbf{n}} \rightarrow 0$, $\frac{1}{M} \|\mathbf{f}_i^H \tilde{\mathbf{n}}\|^2 \rightarrow \frac{\sigma_n^2}{NT_c}$ and $\frac{1}{M} \|\tilde{\mathbf{n}}\|^2 \rightarrow \frac{\sigma_n^2}{NT_c}$, (30)

gives us the result in (13) for $S \leq N$ and is reproduced below

$$Q \approx \zeta \gamma_2 P_t \left(\frac{\gamma_1 \gamma_2 |g|^2 \mu (M+1) + \frac{\gamma_3 N_s^2 \nu}{N_c^2} + \frac{\sigma_n^2 N_s^2}{N_c T_c P_s}}{\gamma_1 \gamma_2 |g|^2 \mu + \gamma_3 \frac{\nu N_s^2}{N_c^2} + \frac{\sigma_n^2 N_s^2}{N_c T_c P_s}} \right). \quad (32)$$

When $N_s = N_c$, (13) simplifies to

$$Q \approx \zeta \gamma_2 P_t \left(\frac{\gamma_1 \gamma_2 |g|^2 \mu (M+1) + \gamma_3 \nu + \frac{\sigma_n^2 N_c}{T_c P_s}}{\gamma_1 \gamma_2 |g|^2 \mu + \gamma_3 \nu + \frac{\sigma_n^2 N_c}{T_c P_s}} \right). \quad (33)$$

Case 2: $N_s \geq N_c$ In this case, $T_s < T_c$. Substituting (1) in (8), we have

$$\mathbf{x}_s = \frac{\sqrt{\gamma_1 \gamma_2} g^* \mathbf{f}^*}{N_c T_c} \int_0^{N_c T_c} \sum_{n=1}^{N_c} c_n^2 p_c^2(t - n T_c) \sqrt{P_s} \sum_{i=1}^{N_s} s_i p_s(t - i T_s) dt, \quad (34a)$$

$$= \sqrt{\gamma_1 \gamma_2 P_s} \frac{g^* \mathbf{f}^*}{N_c T_c} \sum_{n=1}^{N_c} \sum_{i=\frac{N_s}{N_c}(n-1)+1}^{\frac{N_s}{N_c} n} s_i \int_{iT_s}^{(i+1)T_s} p_s(t - iT_s) dt, \quad (34b)$$

$$= \sqrt{\gamma_1 \gamma_2 P_s} \frac{g^* \mathbf{f}^*}{N_c T_c} \sum_{n=1}^{N_c} \sum_{i=\frac{N_s}{N_c}(n-1)+1}^{\frac{N_s}{N_c} n} s_i T_s, \quad (34c)$$

$$= \sqrt{\gamma_1 \gamma_2 P_s} \frac{g^* \mathbf{f}^*}{N_s} \sum_{i=1}^{N_s} s_i, \quad (34d)$$

where the (34c) comes from the fact that $\int_{iT_s}^{(i+1)T_s} p_s(t - iT_s) dt = T_s$ and (34d) is obtained using $N_c T_c = N_s T_s$. Substituting (1) in (9), we obtain

$$\mathbf{x}_i = \frac{\sqrt{\gamma_3} \mathbf{h}^H}{N_c T_c} \int_0^{N_c T_c} \sqrt{P_s} \sum_{i=1}^{N_s} s_i p_s(t - iT_s) \sum_{n=1}^{N_c} c_n p_c(t - nT_c) dt, \quad (35a)$$

$$= \sqrt{\gamma_3 P_s} \frac{\mathbf{h}^H}{N_c T_c} \sum_{n=1}^{N_c} \sum_{i=\frac{N_s}{N_c}(n-1)}^{\frac{N_s}{N_c}n-1} c_n s_i \int_{iT_s}^{(i+1)T_s} p_s(t - iT_s) dt, \quad (35b)$$

$$= \sqrt{\gamma_3 P_s} \frac{\mathbf{h}^H}{N_c T_c} \sum_{n=1}^{N_c} \sum_{i=\frac{N_s}{N_c}(n-1)}^{\frac{N_s}{N_c}n-1} c_n s_i T_s, \quad (35c)$$

$$= \sqrt{\gamma_3 P_s} \frac{\mathbf{h}^H}{N_s} \sum_{n=1}^{N_c} \sum_{i=\frac{N_s}{N_c}(n-1)}^{\frac{N_s}{N_c}n-1} c_n s_i, \quad (35d)$$

where (35c) and (35d) follow from the same reasoning as in (34c) and (34d).

Substituting (34d) and (35d) into (11), we get

$$r_{\text{ER}} = \sqrt{\gamma_2 P_t} \frac{(\frac{\sqrt{\gamma_1 \gamma_2 P_s g}}{N_s} \sum_{i=1}^{N_s} s_i \mathbf{f}^H \mathbf{f} + \frac{\sqrt{\gamma_3 P_s}}{N_s} \sum_{n=1}^{N_c} \sum_{i=\frac{N_s}{N_c}(n-1)+1}^{\frac{N_s}{N_c}n} c_n s_i \mathbf{f}^H \mathbf{h} + \mathbf{f}^H \mathbf{n})}{\left\| \frac{\sqrt{\gamma_1 \gamma_2 P_s g^*}}{N_s} \sum_{i=1}^{N_s} s_i^* \mathbf{f} + \frac{\sqrt{\gamma_3 P_s}}{N_s} \sum_{n=1}^{N_c} \sum_{i=\frac{N_s}{N_c}(n-1)+1}^{\frac{N_s}{N_c}n} c_n s_i^* \mathbf{h} + \mathbf{n} \right\|}. \quad (36)$$

Again substituting (36) in (12) we get:

$$Q = \zeta |r_{\text{ER}}|^2 \approx \zeta \left(\frac{\frac{\gamma_1 \gamma_2^2 P_s P_t |g|^2}{N_s^2} \left| \sum_{i=1}^{N_s} s_i \right|^2 \|\mathbf{f}\|^4 + \frac{\gamma_3 P_s P_t}{N_s^2} \left| \sum_{n=1}^{N_c} \sum_{i=\frac{N_s}{N_c}(n-1)+1}^{\frac{N_s}{N_c}n} c_n s_i \right|^2 \|\mathbf{f}^H \mathbf{h}\|^2 + \gamma_2 P_t \|\mathbf{f}^H \mathbf{n}\|^2}{\frac{\gamma_1 \gamma_2 P_s |g|^2}{N_s^2} \left| \sum_{i=1}^{N_s} s_i^* \right|^2 \|\mathbf{f}\|^2 + \gamma_3 P_s \frac{1}{N_s^2} \left| \sum_{n=1}^{N_c} \sum_{i=\frac{N_s}{N_c}(n-1)+1}^{\frac{N_s}{N_c}n} c_n s_i^* \right|^2 \|\mathbf{h}\|^2 + \|\mathbf{n}\|^2} \right),$$

which, when simplified using the asymptotic Massive MIMO expressions [40], gives the result for $N_s \geq N_c$ in (13), reproduced below:

$$Q \approx \zeta \gamma_2 P_t \left(\frac{\gamma_1 \gamma_2 |g|^2 \mu (M+1) + \gamma_3 \nu + \frac{\sigma_n^2 N_s^2}{N_c T_c P_s}}{\gamma_1 \gamma_2 |g|^2 \mu + \gamma_3 \nu + \frac{\sigma_n^2 N_s^2}{N_c T_c P_s}} \right),$$

where μ and ν are as defined in (31).

APPENDIX B

PROOF OF PROPOSITION 3

In this appendix, we derive the formula for the average harvested energy at the ER during the power transfer phase. When the ambient signal component is cancelled, the instantaneous harvested power at the

ER in (13) simplifies to

$$Q = \zeta \gamma_2 P_t \left(\frac{\gamma_1 \gamma_2 |g|^2 \mu (M+1) + \frac{\sigma_n^2 N_s^2}{N_c T_c P_s}}{\gamma_1 \gamma_2 |g|^2 \mu + \frac{\sigma_n^2 N_s^2}{N_c T_c P_s}} \right). \quad (37)$$

The average harvested energy at the ER is given by

$$\bar{Q} = E[Q] = \int_0^\infty \zeta \gamma_2 P_t \left(\frac{\gamma_1 \gamma_2 z (M+1) + \frac{\sigma_n^2 N_s^2}{N_c T_c P_s}}{\gamma_1 \gamma_2 z + \frac{\sigma_n^2 N_s^2}{N_c T_c P_s}} \right) f_Z(z) dz, \quad (38)$$

where $z = |g|^2 \mu$ and $|g|^2$ and μ are independent of each other. Since $|g|^2 \sim \text{Exp}(1)$ and $\mu \sim \text{Exp}(\frac{1}{N_s})$, $f_Z(z) = \frac{2}{N_s} K_0(2\sqrt{\frac{z}{N_s}})$ for $z \geq 0$, where K_0 is the bessel function of the first kind. Using Mathematica, (38) can be expressed as (20).

REFERENCES

- [1] (2019) IoT Intelligence for Smart Cities. [Online]. Available: <https://www.nnnco.com.au/smart-cities/>
- [2] (22nd November, 2018) World-first smart beaches platform wins \$910,000 Federal grant. [Online]. Available: <https://www.northernbeaches.nsw.gov.au/council/news/media-releases/world-first-smart-beaches-platform-wins-910000-federal-grant/>
- [3] (2019) Agriculture: When farms talk to their farmers. [Online]. Available: <https://www.nnnco.com.au/smart-agriculture/>
- [4] D. N. K. Jayakody, J. Thompson, S. Chatzinotas, and S. Durrani, *Wireless Information and Power Transfer: A New Paradigm for Green Communications*. Springer, 2017.
- [5] K. Huang and X. Zhou, “Cutting the last wires for mobile communications by microwave power transfer,” *IEEE Commun. Mag.*, vol. 53, no. 6, pp. 86–93, 2015.
- [6] S. Bi, C. K. Ho, and R. Zhang, “Wireless powered communication: opportunities and challenges,” *IEEE Commun. Mag.*, vol. 53, no. 4, pp. 117–125, Apr. 2015.
- [7] Y. Zeng, B. Clerckx, and R. Zhang, “Communications and signals design for wireless power transmission,” *IEEE Trans. Commun.*, vol. 65, no. 5, pp. 2264–2290, May. 2017.
- [8] L. Yang, Y. Zeng, and R. Zhang, “Wireless power transfer with hybrid beamforming: How many RF chains do we need?” *IEEE Trans. Wireless Commun.*, vol. 17, no. 10, pp. 6972–6984, Oct. 2018.
- [9] Y. Alsaba, S. K. A. Rahim, and C. Y. Leow, “Beamforming in wireless energy harvesting communications systems: A survey,” *IEEE Commun. Surveys Tuts.*, vol. 20, no. 2, pp. 1329–1360, Secondquarter 2018.
- [10] L. Liu, R. Zhang, and K. Chua, “Multi-antenna wireless powered communication with energy beamforming,” *IEEE Trans. Commun.*, vol. 62, no. 12, pp. 4349–4361, Dec. 2014.
- [11] Y. Zeng and R. Zhang, “Optimized training design for wireless energy transfer,” *IEEE Trans. Commun.*, vol. 63, no. 2, pp. 536–550, Feb. 2015.
- [12] —, “Optimized training for net energy maximization in multi-antenna wireless energy transfer over frequency-selective channel,” *IEEE Trans. Commun.*, vol. 63, no. 6, pp. 2360–2373, June 2015.

- [13] G. Yang, C. K. Ho, and Y. L. Guan, "Dynamic resource allocation for multiple-antenna wireless power transfer," *IEEE Trans. Signal Process.*, vol. 62, no. 14, pp. 3565–3577, July 2014.
- [14] X. Chen, C. Yuen, and Z. Zhang, "Wireless energy and information transfer tradeoff for limited-feedback multiantenna systems with energy beamforming," *IEEE Trans. Veh. Technol.*, vol. 63, no. 1, pp. 407–412, Jan. 2014.
- [15] H. Son and B. Clerckx, "Joint beamforming design for multi-user wireless information and power transfer," *IEEE Trans. Wireless Commun.*, vol. 13, no. 11, pp. 6397–6409, Nov. 2014.
- [16] J. Park and B. Clerckx, "Joint wireless information and energy transfer with reduced feedback in MIMO interference channels," *IEEE J. Sel. Areas Commun.*, vol. 33, no. 8, pp. 1563–1577, Aug. 2015.
- [17] J. Xu and R. Zhang, "Energy beamforming with one-bit feedback," *IEEE Trans. Signal Process.*, vol. 62, no. 20, pp. 5370–5381, Oct. 2014.
- [18] Y. Zeng and R. Zhang, "Optimized training design for wireless energy transfer," *IEEE Trans. Commun.*, vol. 63, no. 2, pp. 536–550, Feb. 2015.
- [19] S. Lee, Y. Zeng, and R. Zhang, "Retrodirective multi-user wireless power transfer with massive MIMO," *IEEE Commun. Lett.*, vol. 7, no. 1, pp. 54–57, Feb. 2018.
- [20] I. Krikidis, "Retrodirective large antenna energy beamforming in backscatter multi-user networks," *IEEE Commun. Lett.*, vol. 7, no. 4, pp. 678–681, Feb. 2018.
- [21] R. Y. Miyamoto and T. Itoh, "Retrodirective arrays for wireless communications," *IEEE Microw. Mag.*, vol. 3, no. 1, pp. 71–79, Mar. 2002.
- [22] G. Yang, C. K. Ho, and Y. L. Guan, "Multi-antenna wireless energy transfer for backscatter communication systems," *IEEE J. Sel. Areas Commun.*, vol. 33, no. 12, pp. 2974–2987, Dec. 2015.
- [23] N. Van Huynh, D. T. Hoang, X. Lu, D. Niyato, P. Wang, and D. I. Kim, "Ambient backscatter communications: A contemporary survey," *IEEE Commun. Surveys Tuts.*, vol. 20, no. 4, pp. 2889–2922, 4th Quart. 2018.
- [24] W. Liu, K. Huang, X. Zhou, and S. Durrani, "Next generation backscatter communication: systems, techniques, and applications," *EURASIP Journal on Wireless Commun. and Netw.*, vol. 69, pp. 1–11, Mar. 2019.
- [25] V. Liu, A. Parks, V. Talla, S. Gollakota, D. Wetherall, and J. R. Smith, "Ambient backscatter: wireless communication out of thin air," in *Proc. ACM SIGCOMM*, vol. 43, no. 4. ACM, 2013, pp. 39–50.
- [26] A. N. Parks, A. Liu, S. Gollakota, and J. R. Smith, "Turbocharging ambient backscatter communication," *Proc. ACM SIGCOMM*, vol. 44, no. 4, pp. 619–630, 2015.
- [27] J. Kimionis, A. Bletsas, and J. N. Sahalos, "Increased range bistatic scatter radio," *IEEE Trans. Commun.*, vol. 62, no. 3, pp. 1091–1104, Mar. 2014.
- [28] G. Wang, F. Gao, R. Fan, and C. Tellambura, "Ambient backscatter communication systems: Detection and performance analysis," *IEEE Trans. Commun.*, vol. 64, no. 11, pp. 4836–4846, Nov. 2016.
- [29] J. Qian, F. Gao, G. Wang, S. Jin, and H. Zhu, "Noncoherent detections for ambient backscatter system," *IEEE Trans. Wireless Commun.*, vol. 16, no. 3, pp. 1412–1422, Mar. 2017.
- [30] B. Kellogg, V. Talla, S. Gollakota, and J. R. Smith, "Passive WI-FI: Bringing low power to wi-fi transmissions," in *Proc. 13th Symp.*

Netw. Syst. Design Implementation, 2016, pp. 151–164.

- [31] G. Yang, Y. Liang, R. Zhang, and Y. Pei, “Modulation in the air: Backscatter communication over ambient ofdm carrier,” *IEEE Trans. Commun.*, vol. 66, no. 3, pp. 1219–1233, Mar. 2018.
- [32] P. Zhang, M. Rostami, P. Hu, and D. Ganesan, “Enabling practical backscatter communication for on-body sensors,” in *Proc. ACM SIGCOMM*, 2016, pp. 370–383.
- [33] V. Iyer, V. Talla, B. Kellogg, S. Gollakota, and J. Smith, “Inter-technology backscatter: Towards internet connectivity for implanted devices,” in *Proc. ACM SIGCOMM*, 2016, pp. 356–369.
- [34] D. Bharadia, K. R. Joshi, M. Kotaru, and S. Katti, “BackFi: High throughput Wi-Fi backscatter,” *ACM SIGCOMM Comput. Commun. Review*, vol. 45, no. 4, pp. 283–296, 2015.
- [35] P. Zhang, D. Bharadia, K. Joshi, and S. Katti, “Hitchhike: Practical backscatter using commodity wifi,” in *Proc. ACM Conf. Embedded Netw. Sensor Syst.* ACM, 2016, pp. 259–271.
- [36] I. S. Gradshteyn and I. M. Ryzhik, *Table of integrals, series, and products*, 7th ed. Elsevier/Academic Press, Amsterdam, 2007.
- [37] C. Pon, “Retrodirective array using the heterodyne technique,” *IEEE Trans. Antennas Propag.*, vol. 12, no. 2, pp. 176–180, Mar. 1964.
- [38] Q. Tao, C. Zhong, H. Lin, and Z. Zhang, “Symbol detection of ambient backscatter systems with manchester coding,” *IEEE Trans. Wireless Commun.*, vol. 17, no. 6, pp. 4028–4038, Jun. 2018.
- [39] A. Goldsmith, *Wireless Communications*. Cambridge University Press, 2005.
- [40] Y. Lim, C. Chae, and G. Caire, “Performance analysis of massive MIMO for cell-boundary users,” *IEEE Trans. Wireless Commun.*, vol. 14, no. 12, pp. 6827–6842, Dec. 2015.